Journal Name

ARTICLE TYPE

Cite this: DOI: 00.0000/xxxxxxxxxx

Supplementary Information: Effects of Shear Flow on Structure and Dynamics of Ionic Liquid in Metallic Nanoconfinement

Samuel Ntim and Marialore Sulpizi*

Received Date
Accepted Date

DOI: 00.0000/xxxxxxxxxx

Contents

S1 Density and interfacial structure

Apart from narrowing of the peaks from shearing, the interface is predominantly unchanged in its structure. This is exemplified by the density profile of the anions in Figure 4 where the system is at a shear velocity of $v_{\text{slab}} = \pm 10\,\text{m}\,\text{s}^{-1}$. Similarly, at a velocity of $v_{\text{slab}} = \pm 20\,\text{m}\,\text{s}^{-1}$, the interfacial structure shown in Figures S1, S2 and S3 remains essentially identical to that of an equilibrium system.

S2 Orientation of cations

We describe further the interfacial structure by looking at the orientation of the cations. Just has already been discussed in the main text, the cations, to a significant extent, retain their equilibrium orientation. This is so, irrespective of shearing velocity and temperature as demostrated by the distributions of angles in Figures S4, S5, S6, S7 and S8.

Institut für Physik, Johannes Gutenberg Universität, Staudingerweg 7, 55128-Mainz, Germany; E-mail: sulpizi@uni-mainz.de

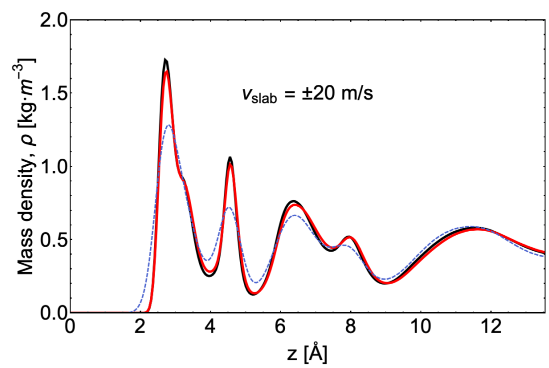

Fig. S1 Denstity profile of anions at slab velocity of $\pm 20\,\text{m}\,\text{s}^{-1}$. The blue dashed line represents the density profile of anions at 298 K at equilibrium, where no shear is applied and the thermostat is applied to the whole system.

S3 Steinhardt order parameter

We calculated the global Steinhardt order by averaging the local orientational order parameter for the ith atom

$$q_6(i) = \sqrt{\frac{4\pi}{13} \sum_{m=-6}^{6} |q_{6m}(i)|^2} \tag{1}$$

where $q_{6m}(i)$ are components of a 13-dimensional complex vector, used to describe the locality of ith atom. It is defined as

$$q_{6m}(i) = \frac{1}{N_{nn}(i)} \sum_{j=1}^{N_{nn}(i)} Y_{6m}(\theta_{ij}, \phi_{ij}) \tag{2}$$

which is an average over all nearest neighbours of the ith atom, $N_{nn}(i)$ of the spherical harmonics $Y_{6m}(\theta_{ij}, \phi_{ij})$ of polar and azimuthal angles θ_{ij} and ϕ_{ij} made by the vector $\mathbf{r}_{ij}$ to some reference coordinate. The global order parameter Q_6 is then calculated as the average of $q_6(i)$ over all atoms.

Figures S9 and S10 show the Q_6 profiles at slab velocities of

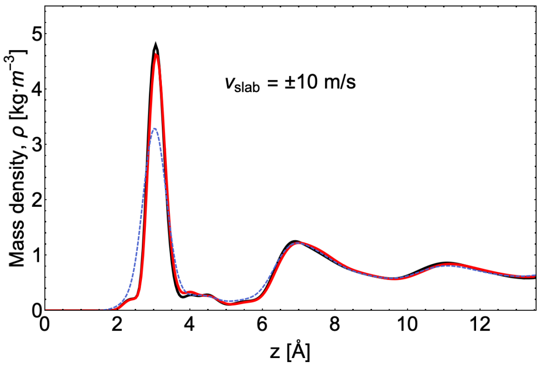

Fig. S2 Denstity profile of cations at slab velocity of $\pm 10\,\mathrm{m\,s^{-1}}$. The blue dashed line represents the density profile of cations at $298\,\mathrm{K}$ and without shear, and with the whole system connected to the thermostat.

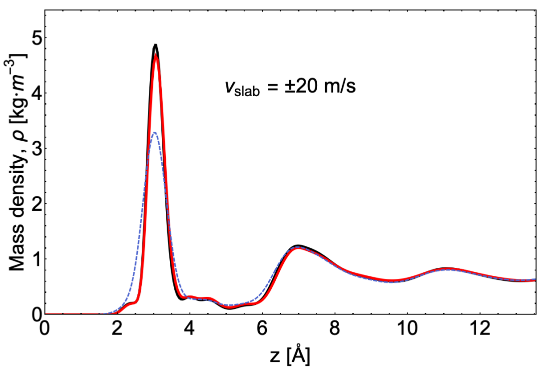

Fig. S3 Denstity profile of cations at slab velocity of $\pm 20\,\mathrm{m\,s^{-1}}$. The blue dashed line represents the density profile of cations at $298\,\mathrm{K}$ and without shear.

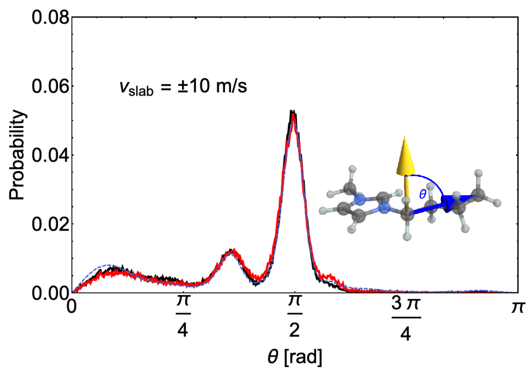

Fig. S4 Distribution of angle made by cation tail at the interface at slab velocity of $\pm 10\,\mathrm{m\,s^{-1}}$. The blue dashed line represents that with the whole system thermostatted at $298\,\mathrm{K}$ and without shear.

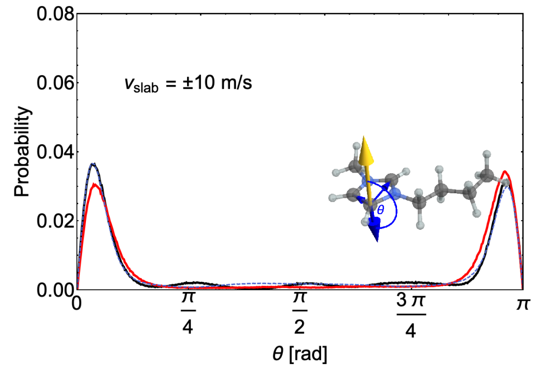

Fig. S5 Distribution of angle made by plane of imidazolium ring at the interface at slab velocity of $\pm 10\,\mathrm{m\,s^{-1}}$. The blue dashed line represents that at $298\,\mathrm{K}$ and without shear.

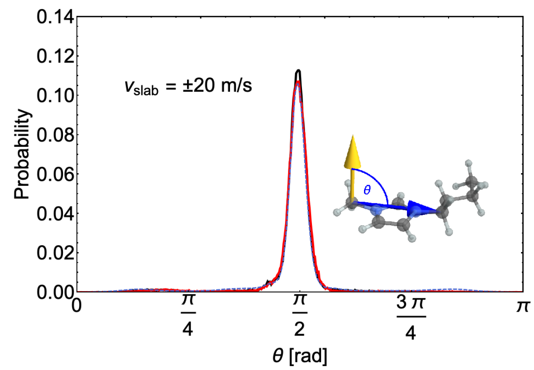

Fig. S6 Distribution of angle made by the axis through the imidazolium, at the interface with slab velocity of $\pm 20\,\mathrm{m\,s^{-1}}$. The blue dashed line represents the same distribution with the whole system thermostatted at $298\,\mathrm{K}$ in equilibrium.

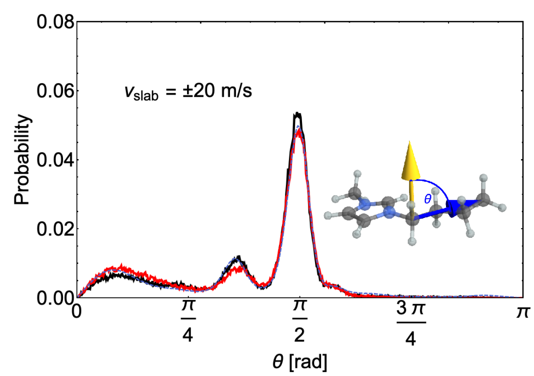

Fig. S7 Distribution of angle made by cation tail at the interface at slab velocity of $\pm 20\,\mathrm{m\,s^{-1}}$. The blue dashed line represents the same distribution at $298\,\mathrm{K}$ and without shear.

$10\,\mathrm{m\,s^{-1}}$ and $20\,\mathrm{m\,s^{-1}}$, respectively, at the two temperature levels. The temperature profiles are only included to demonstrate the parabolic nature of the Q_6 profile.

S4 Shear viscosity and shear thinning

We show in the following tables the shear viscosity at different slab velocities calculated for the whole cavity of ionic liquid bounded by $\pm 118.575\,\mathrm{Å}$ and for the midsection bounded by $\pm 20\,\mathrm{Å}$ where we observe ideal Couette flow. We report also the velocities at these bounds and the average temperature within the bounds.

In our simulations, we have the flow of the liquid in the direction y and a velocity gradient in the direction z. We calculate the shear viscosities from the components in these directions of average pressure tensor in the corresponding region R and the shear rate $\dot{\gamma}_R$ using the velocity v_B at the boundary to that region in this way:

$$\eta_R = -\frac{\langle P_{yz} \rangle}{\dot{\gamma}_R} \tag{3}$$

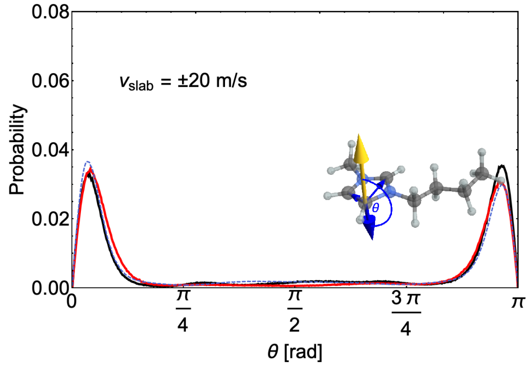

Fig. S8 Distribution of angle made by plane of imidazolium ring at the interface at slab velocity of $\pm 20\,\mathrm{m\,s^{-1}}$. The blue dashed line represents that at 298 K and without shear.

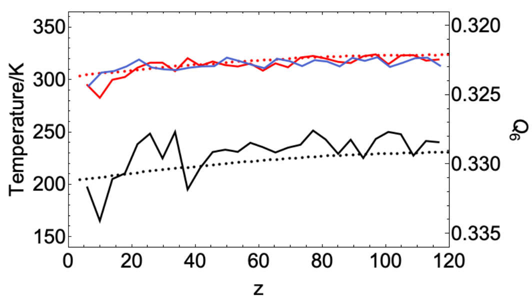

Fig. S9 Q_6 and temperature profiles at $\pm 10\,\mathrm{m\,s^{-1}}$ slab velocity. Dotted curves represent temperature profiles while joined curves represent the Q_6 profiles. The blue is the Q_6 profile for an equilibrium system thermostatted at 298 K.

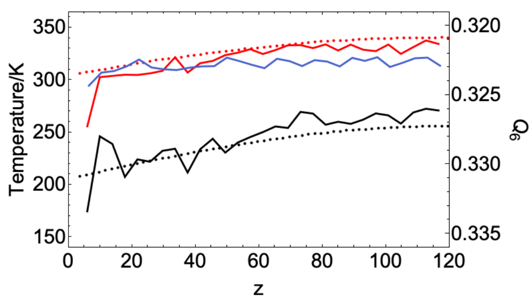

Fig. S10 Q_6 at $\pm 20\,\mathrm{m\,s^{-1}}$ slab velocity. Dotted curves represent temperature profiles while joined curves represent the Q_6 profiles. The blue is the Q_6 profile for an equilibrium system thermostatted at 298 K.

where $\dot{\gamma}_R = \frac{2\times v_B}{h_R}$, h_R being the thickness of the region R.

Table SI Boundary velocity, average temperature and viscosity at slab velocity $\pm 10\,\mathrm{m\,s^{-1}}$ for low and high temperatures.

Bounds/Å	Low temperature			High temperature		
	$v_B/\mathrm{m\,s^{-1}}$	$\bar{T}/\mathrm{K}$	$\eta/\mathrm{mPa\cdot s}$	$v_B/\mathrm{m\,s^{-1}}$	$\bar{T}/\mathrm{K}$	$\eta/\mathrm{mPa\cdot s}$
±20.0	2.8	229.2	14.3	2.4	323.3	9.9
±118.575	10.0	202.1	22.7	10.0	302.4	17.9

Table SII Boundary velocity, average temperature and viscosity at slab velocity $\pm 20\,\mathrm{m\,s^{-1}}$ for low and high temperatures.

Bounds/Å	Low temperature			High temperature		
	$v_B/\mathrm{m\,s^{-1}}$	$\bar{T}/\mathrm{K}$	$\eta/\mathrm{mPa\cdot s}$	$v_B/\mathrm{m\,s^{-1}}$	$\bar{T}/\mathrm{K}$	$\eta/\mathrm{mPa\cdot s}$
±20.0	6.3	253.0	6.7	4.8	339.2	6.3
±118.575	20.0	202.9	12.3	20.0	303.6	8.2

S5 Pressure in "frozen" layer and normal stress coefficients

We show here in Table SIII a comparison of the average pressure in the "frozen" layer to that of the rest of the liquid for all our simulations. The pressure in a region is calculated from the average pressure tensor **P** of all atoms in that region as

$$p = \frac{1}{3V}\mathrm{Tr}(\mathbf{P}) \tag{4}$$

where V is the volume of the region under consideration.
The average differences in normal stress coefficients are crucial in determining whether or not the liquid is readily deformable in certain direction—whether or not the liquid is Newtonian. However, it necessary to have a converge pressure tensor. In Fig. S11 we show an example convergence of the diagonal components of the pressure tensor and their total, over time, for our low temperature system at $10\,\mathrm{m\,s^{-1}}$ slab velocity.

Table SIII Average pressure in "frozen" layer p_f $(0 < z \leq \lambda)$ in comparison with average pressure of rest of ionic liquid p_r $(|z| < \lambda)$.

$v_{\text{slab}}/\mathrm{m\,s^{-1}}$	Low temp.			High temp.		
	λ/Å	p_f/MPa	p_r/MPa	λ/Å	p_f/MPa	p_r/MPa
10	10.60	−344.01	−100.44	5.96	−337.10	47.08
20	16.51	−257.19	−74.91	6.49	−281.27	73.77

The first and second normal stress coefficients are defined here as

$$\psi_1 = \frac{\langle P_{zz} - P_{yy}\rangle}{\dot{\gamma}^2} \tag{5}$$

and

$$\psi_2 = \frac{\langle P_{xx} - P_{zz}\rangle}{\dot{\gamma}^2} \tag{6}$$

Table SIV shows the normal stress coefficients and their ratios, calculated from the diagonal elements of the pressure tensor according to these equations.

S6 Load and friction

We increased the load on the ionic liquid by moving the each gold slab in steps of 0.5 Å towards the other every 10 ps until the desired reduction in the slab separation is reached, and then a run of 52 ns. For a given slab separation reduction of s the load

Table SIV Average first and second normal stress coefficients, and their ratios at low and high temperatures.

$v_{slab}/\mathrm{m\,s^{-1}}$	Low temp.			High temp.		
	$\psi_1/\mathrm{pPa\,s^2}$	$\psi_2/\mathrm{pPa\,s^2}$	$\frac{-\psi_2}{\psi_1}$	$\psi_1/\mathrm{pPa\,s^2}$	$\psi_2/\mathrm{pPa\,s^2}$	$\frac{-\psi_2}{\psi_1}$
10	1050.88	−653.16	0.62	935.25	−555.63	0.59
20	265.15	−164.93	0.62	235.33	−138.66	0.59

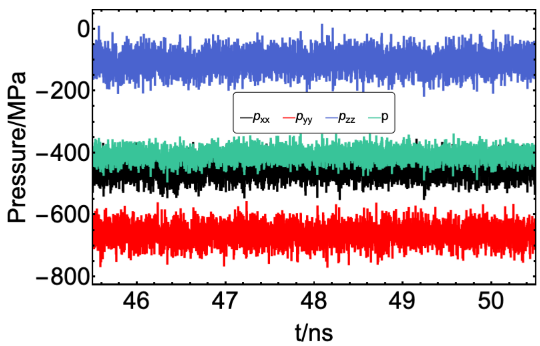

Fig. S11 Convergence of the diagonal components of the pressure tensor for lower temperature system with slab velocity of $\pm 10\,\mathrm{m\,s^{-1}}$.

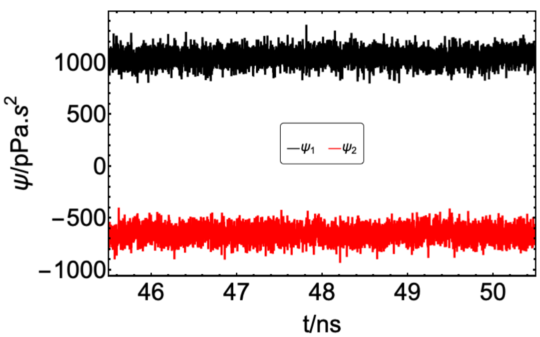

Fig. S12 Convergence of ψ_1 and ψ_2 for lower temperature system with slab velocity of $\pm 10\,\mathrm{m\,s^{-1}}$.

L_s corresponding to a slab separation of $h = h_0 - s$ where h_0 is the equilibrium slab separation, is calculated by difference in the average normal forces on the slabs. The average force on the lower slab, say, is calculate every 1 ps as

$$F^{\text{lower}} = \sum_{i \in \text{lower}} \langle \mathbf{f}_i(t) \rangle \tag{7}$$

then the load per area is evaluated as $f_L = 0.5 \times (F_z^{\text{upper}} - F_z^{\text{lower}})/(L_x L_y)$. Table SV shows the load at different temperatures, velocities and slab separations. Figures S13 to S16 show the density profiles at the smallest slab separation simulated, $h_0 - 12\,\text{Å}$. The dashed lines indicate the corresponding density profiles at slab separation of h_0.

Table SV Load on systems. Each L_s is the load for system with slab separation $h = h_0 - s$ where $h_0 = 237.15\,\text{Å}$.

$v_{slab}/\mathrm{m\,s^{-1}}$	Low temperature			High temperature		
	L_0/GPa	L_6/GPa	L_{12}/GPa	L_0/GPa	L_6/GPa	L_{12}/GPa
10	−0.09	−0.01	0.09	0.06	0.15	0.27
20	−0.07	0.02	0.12	0.08	0.17	0.32

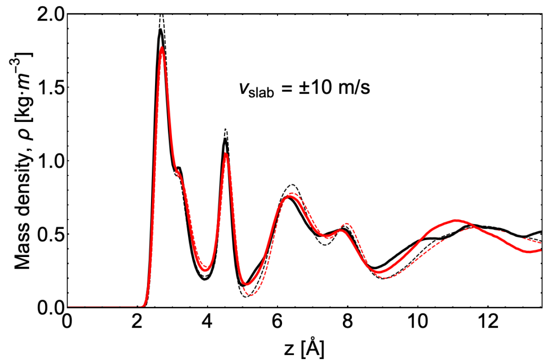

Fig. S13 Density profile of anions at slab velocity of $\pm 10\,\mathrm{m\,s^{-1}}$ at slab separation of $h_0 - 12\,\text{Å}$ The dashed line represents the corresponding density profile of anions at slab separation of h_0.

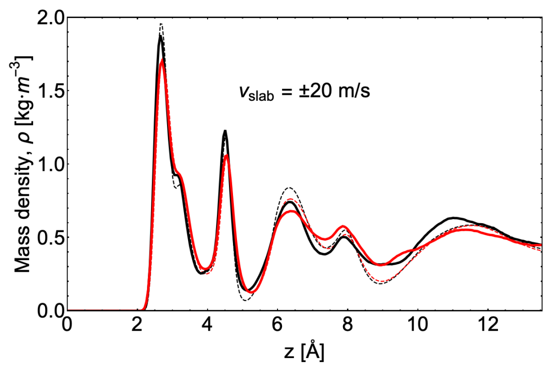

Fig. S14 Density profile of anions at slab velocity of $\pm 20\,\mathrm{m\,s^{-1}}$ at slab separation of $h_0 - 12\,\text{Å}$ The dashed line represents the corresponding density profile of anions at slab separation of h_0.

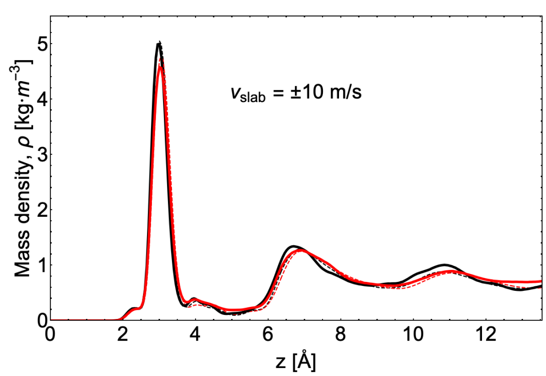

Fig. S15 Density profile of cations at slab velocity of $\pm 10\,\mathrm{m\,s^{-1}}$ at slab separation of $h_0 - 12\,\text{Å}$ The dashed line represents the corresponding density profile of cations at slab separation of h_0.

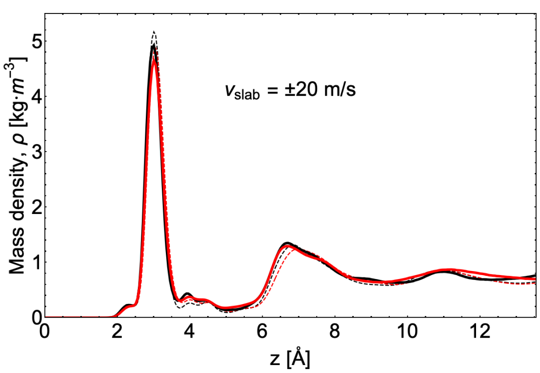

Fig. S16 Density profile of cations at slab velocity of $\pm 20\,\mathrm{m\,s^{-1}}$ at slab separation of $h_0 - 12\,\text{Å}$ The dashed line represents the corresponding density profile of cations at slab separation of h_0.